CAAP Annual Report

Date of Report: *09/30/2024*

Prepared for: *U.S. DOT Pipeline and Hazardous Materials Safety Administration*

Annual Period: **From** *(10, 01, 2023)* **to** *(09, 30, 2024)*

Contract Number: *693JK3215002CAAP*

Project Title: *Easy Deployed Distributed Acoustic Sensing System for Remotely Assessing Potential and Existing Risks to Pipeline Integrity*

Prepared by: *Yilin Fan, Ge Jin, Ali Tura, Jennifer Miskimins*

Contact Info.: *yilinfan@mines.edu, 303-273-3749*

Table of Contents

Section A: Business and Activities

(a) Contract Activities

- Contract Modifications:

  The project has been granted a no-cost extension for 12-month period. With that, the project will end on 09/30/2025. The budget narrative has been modified accordingly, detailing the use of the remaining funds. It has been approved by the agreement officer (AO), and the contract has been updated.

- Educational Activities:

  - Student mentoring:

    Two Ph.D. students are fully engaged in this project since 2021S. They are:

    1. Ana Garcia-Ceballos, Ph.D. student in Geophysics
    2. Mouna-Keltoum Benabid, Ph.D. student in Petroleum Engineering

    In addition, various students have been involved in this project and offered temporary support to this project as needed. The students who have made substantial contributions to this project in this reporting year include:

    1. Peyton Baumgartner, Undergraduate student in Petroleum Engineering at Colorado School of Mines, supported this project on the experimental program.
    2. Raad Al-saifi, Undergraduate student in Petroleum Engineering at Colorado School of Mines, supported this project in the experimental program.
    3. Binghao Li, Undergraduate student in Geophysics at University of Science and Technology of China, did an internship at Colorado School of Mines and supported this project on data processing and in the experimental program.

  - Student internship:

    In 2024 Summer, both Mouna-Keltoum Benabid and Ana Garcia-Ceballos did an internship at BP.

  - Educational activities:

    During the past period, we educated the students who have been participating in this project on relevant pipeline integrity problems and diagnosis technologies.

  - Career employed:

    None.

  - Others:

None.

- Dissemination of Project Outcomes:

    1. 1 Journal paper under review:

        Submitted a journal paper to SPE Journal, which is currently under review. The content is from Task#2 from this project. Details are:

        Garcia-Ceballos, A., Benabid, M-K., Jin, G., and Fan, Y. "Monitoring Slug Flow Using Distributed Acoustic Sensing Technology with Different Sensing Cables". Submitted to SPE Journal. Under "Major Revision" (the first decision).

    2. 1 full-length conference proceeding:

        Presented the outcomes from Task#6 at the SPE Annual Technical Conference and Exhibition. Published a full-length conference proceeding:

        Benabid, M-K., Garcia-Ceballos, A., Jin, G., and Fan, Y. "Easy Deployed Distributed Acoustic Sensing System for Leakage Detection in Gas Pipelines". Presented at SPE Annual Technical Conference and Exhibition, 23 – 25 September 2024, New Orleans, Louisiana, USA. https://doi.org/10.2118/220999-MS

    3. 2 other presentations:

        1) Presented at SPE Annual Technical Conference and Exhibition as a panelist, 23 – 25 September 2024, New Orleans, Louisiana, USA. Special session: "Distributed Fiber Optic Sensing – Flow Measurement Perspective". Title: "*Slug Flow Characterization and Monitoring Using Distributed Acoustic Sensing*".

        2) Presented in workshop: *Fan, Y., Jin, G., Garcia-Ceballos, A., Benabid, M-K. "Monitoring of Multiphase Flow and Liquid Loading in Hilly-Terrain Pipelines and Horizontal Wells using Distributed Acoustic Sensing Technology". Presented at SPE Workshop: Fiber-Optic Sensing Applications for Well, Reservoir and Asset Management, 30–31 July 2024, San Luis Resort, Galveston Texas, US.*

        3) Presented at IMAGE 2024 as student poster: *Garcia-Ceballos, A., Benabid, M-K. Jin, G., Fan, Y., " Slug flow monitoring using distributed acoustic sensing in pipelines or horizontal wells". Presented at IMAGE 2024, 26–29 August 2024, Houston, Texas, US.*

- Citations of The Publications:

    None.

- Others:

    None.

(b) Financial Summary (this part will be updated later)

This financial summary was prepared on 9/29/23. Please note that the actual amount in the final annual financial report might be slightly different from the numbers shown below, since some of the expenses occurring in late the year may not be shown in the university's financial system that we use for managing the funds and expenses by the time the report is submitted. Normally, it takes several days for an expense to be shown in the system after its occurrence.

- Federal Cost Activities:
  - PI/Co-PIs/students involvement:

    The table below summaries the expenses for PI/Co-PIs/Students during the past year:

Items\Budget and Expenses		Expenses
1	Faculty Salaries, Wages, and Fringe Benefits	$29,031.37
2	Student Salaries	$41,316.63
3	Graduate Student Tuition	$29,785.50

  - Materials purchased/travel/contractual (consultants/subcontractors):

Items\Budget and Expenses		Expenses
1	Experimental Expenses (experimental work supplies, services, maintenance, cables, air compressor operations, etc.)	$6,112.36
2	Travel	$4,375.09

    The indirect cost in the past year is around $41,630.26.

    The total expense is around $152,251.21.

- Cost Share Activities:
  - Cost share contribution: The cost share is the AY efforts of the PI and co-PIs, that makes up 20% of the total expenses.

(c) Project Schedule Update

- Project Schedule:

  Due to various reasons, we'll need some additional time to fully complete the project objectives and ensure the successful conclusion of our research. Nevertheless, we have tried our best to stay on track with our research work. We have completed most of our tasks, except the two tests for the "unburied" case in Task#3, and the "buried" cases for Tasks#3,4 and 6. We anticipate completing these tasks soon, as the construction of the facility is nearly finished. Below is the updated timeline for the project. We are very optimistic that, with a 12-month extension, the project will be successfully completed.

Tasks	Year 1				Year 2				Year 3				Year 4			
	Q1	Q2	Q3	Q4	Q5	Q6	Q7	Q8	Q9	Q10	Q11	Q12	Q13	Q14	Q15	Q16
	2021	2022				2023				2024				2024		
	O-D	J-M	A-J	J-S	O-D	J-M	A-J	J-S	O-D	J-M	A-J	J-S	O-D	J-M	A-J	J-S
Task#1. Detection of Liquid Accumulation at Pipeline Lower Spots																
1.1 Facility modification and preparation																
1.2 Flow loop test without liquid accumulation																
1.3 Flow loop tests with liquid accumulation																
Task#2. Detection of Dynamic Intermittent (Slug) Structure																
2.1 Flow loop tests with Interminttent Structure																
Task#3. Detection of Corroded Spots on Pipeline Interior																
3.1 Facility modification and preparation																
3.2 Lab tests of corrosion using speciman																
3.3 Flow loop test in buried pipe																
3.4 Flow loop test in unburied pipe																
3.5 Flow loop test in densely supported pipe						densely or sparsely supported						unburied		buried		
3.6 Flow loop test in sparsely supported pipe																
Task#4. Detection of Dent/Deformation on Pipeline																
4.1 Flow loop test in buried pipe																
4.2 Flow loop test in sparsely supported pipe																
Task#5. Detection of Infrastructure Damage																
5.1 Flow loop test in densely supported pipe																
5.2 Flow loop test in sparsely supported pipe																
Task#6. Detection of Leakage																
6.1 Flow loop test in buried pipe																
6.2 Flow loop test in sparsely supported pipe																
Final Report Preparation																
Publication																

- Corrective Actions:

  A 12-month no-cost extension has been submitted and approved.

(d) Status Update of the 12th Quarter Technical Activities

- Task 1: Detection of Liquid Accumulation at Pipeline Lower Spots

  This task has been completed by the 6th quarter.

- Task 2: Detection of Dynamic Intermittent (Slug) Structure

  This task has been completed by the 10th quarter. In the 12th quarter, we worked on revising the manuscript submitted to SPE Journal, according to the comments from the reviewers.

- Task 3: Detection of Corroded Spots on Pipeline Interior Surface

  During the 12th quarter, we completed the processing and analysis of the data for the three corroded pipes that were tested in the 11th quarter, which included pipes with 3 mm and 5 mm corroded depths, as well as a severely corroded pipe with a minor leak. We conducted experiments on all three pipes, testing five different flow rates (2, 6, 10, 14, 18 m/s). The resulting data were compared to experiments conducted on the central 1-meter section of the pipe without defects, serving as our baseline or control experiment in the data processing workflow section. Additionally, we tested two pipe installation configurations (5 and 4 supports) in the repeated experiments. Our experimental results showed that the presence of corrosion inside the 3 mm and 5 mm corroded pipes were hardly detectable. However, we were able to detect corrosion in the severely corroded pipe. In the future, we will explore more deeply with different data processing algorithms to further investigate the cable detectability on these less corroded pipes.

- Task 4: Detection of Dent/Deformation on Pipeline

  During the 12th quarter, we processed and analyzed the data from the repeated experiments on two dented pipes, completed in the previous quarter. One pipe exhibited substantial deformation, simulating a significant structural compromise, while the other presented a smaller dent, representing a less severe scenario. These experiments were conducted under the same five flow rates (2, 6, 10, 14, 18 m/s) and were compared against the control experiment on the central 1-meter section of a defect-free pipe. We also tested two pipe installation configurations (5 and 4 supports), consistent with the methodology applied in Task#3. The purpose of repeating the experiments for both dent sizes was to validate our previous findings and ensure the robustness of the results. The repeated experiments confirmed the previous observations.

- Task 5: Detection of Infrastructure Damage

  In this task, part of the infrastructure damage investigation, we utilized an intact and defect-free central 1-meter section of the pipeline. The primary modification involved varying the number of tripods supporting the pipeline. In contrast to previous tests, we initially used five evenly distributed supports along the pipeline and then removed the support located at the center, corresponding to the middle of the 1-meter test section, to simulate support damage. The repeated tests confirmed the previous observations.

- Task 6: Detection of Leakage

  The leakage tests in supported pipes were extensively done in the 8th and 9th quarters, and the results were discussed in the corresponding quarterly reports. More details are also provided in this annual report in the "Results and Discussion" section. A full-length conference proceeding, discussing the outcomes from this task, was published during this period, which is listed in the publication section.

Section B: Detailed Technical Results in the Report Period

1. Background and Objectives in the 2nd Annual Report Period

1.1. Background

There are more than 220,000 miles of hazardous liquid or carbon dioxide pipeline system and 320,000 natural gas transmission and gathering pipelines traverse the United States as of 2019 according to the latest annual report from U.S. Department of Transportation Pipeline and Hazardous Materials Safety Administration. Reliable assessment of pipeline integrity is of greatest importance to the environment, economy, and society. Pipeline failure can be induced by various sources, such as internal or external corrosion (including microbiologically influenced corrosion), stress corrosion cracking, material/weld failure, excavation damage, incorrect operations, and natural force damages (i.e., seismic events, flooding, lightning, etc.).

Some widely used and/or studied pipeline integrity assessment techniques include in-line inspection (ILI) tools, such as "smart pigs" and robots, and hydrostatic pressure tests. ILI tools travel through the pipe and measure and record irregularities that may represent corrosion, cracks, laminations, deformations (dents, gouges, etc.), or other defects [1]. However, these tools are not always applicable to pipelines. They also require pipeline operators to periodically conduct investigations, which consumes an enormous amount of time and affects oil and gas transportation [2]. Hydrostatic pressure tests can pose additional risks to the pipeline integrity, such as flaw growth [3], pipeline rupture [4], or other potential component failure [5].

Distributed Fiber-Optic Sensing (DFOS) is a recent trending technology for remote pipeline integrity monitoring. By connecting the instrument to one end of a regular telecommunication fiber, DFOS systems can take distributed measurements along the fiber with high spatial and temporal resolution. Modern system development allows a single instrument to measure more than 50-km of fiber simultaneously [6], which is highly cost-effective for pipeline monitoring purposes. DFOS systems include Distributed Acoustic Sensing (DAS), Distributed Temperature Sensing (DTS), and Distributed Strain Sensing (DSS).

Compared with other technologies such as ILI and pressure tests, DFOS has established many advantages in several aspects. First, it can provide continuous monitoring of pipeline operating conditions and remote detection of leaks [7] without disturbing production and operation, while most other technologies provide one-time investigation and require operators to conduct assessments periodically. The continuous monitoring also enables the operators to track the changes in operation conditions (such as pressure cyclic events that can lead to a faster cracking) and potentially the change/growth of existing threats with time, which can significantly promote the fundamental understanding of crack growth rate with operating conditions and/or environment. Second, DFOS provides real-time monitoring and can provide quick responses in remote areas without waiting for days after the leaks dramatically occur, such that the operators can take immediate actions to avoid catastrophic damage due to late responses. It can also detect and localize any anomaly due to natural forces and human intrusion, such that the operators will be more cautious about potential threats in that area.

Many works have been done to investigate the feasibility of using DFOS systems for pipeline monitoring applications. Early studies demonstrated that by placing the sensing fiber cable underneath or close to the pipeline, DTS can detect and locate anomalous temperature variations induced by fluid or gas leakage [8–10]. If the fiber is mechanically coupled to the pipeline using glue, tape, or clamp, bending and deformation of the pipeline infrastructure can also be detected [2,11]. One of the previous studies [12] showcased a long-term field pipeline monitoring program using DTS and DSS where leakage, landslide, and surface subsidence events were successfully detected and monitored.

Besides DTS and DSS, DAS is capable of monitoring vibrations of and near the pipelines, with high temporal and spatial resolutions. By sending a coherent laser pulse into the fiber, DAS interrogator measures the phase changes of the back-scattered laser energy, which can then be converted to distributed strain rate measurements. A typical DAS instrument can measure more than 6000 locations (channels) simultaneously, with a temporal sampling rate of more than 10 kHz (fiber length dependent), making it an ideal tool to monitor pipeline vibrations remotely and in real-time.

The usage of DAS for pipeline monitoring has also been investigated in recent years. Tejedor et al. [13] demonstrate that using DAS signal detect pipeline intrusion events. Stajanca et al. [14] show that DAS signal is also sensitive to leakage-related vibrations. However, the study was not able to separate the pipe infrastructure vibrations from the vibrations induced by leakage, especially in the high pressure, high flow rate examples. A more recent study characterized leakage noise for buried gas pipelines, measured using different DAS cable designs [7]. The experiment was set up to minimize the pipeline vibrations so the recorded data were dominated by leakage signals.

Most of the previous studies focus on leakage or intrusion-induced vibrations, and treat pipeline vibration induced by flow as unwanted and environmental “noise”. However, flow-induced vibrations contain critical information for pipeline health and risk assessment. Large pipeline vibrations may be related to improper pipeline installation, damaged supporting infrastructure, or unwanted slug flow within the pipeline. Prolonged vibrations may also compromise the life span of the infrastructure, and increase the risk of external corrosion and damage at the joint and supporting/contact points.

The flow-induced pipeline vibration has been intensively studied in the past several decades [15–18]. It is not the intention of this proposal to repeat or extend previous research to understand the fundamental physics of vibrations. Rather, we focus on understanding the flow-induced vibrations that are associated with potential risks for pipeline integrity, and how these vibrations interact with sensing fiber cables.

Sensing fiber installation along the pipeline significantly affects the cost and effectiveness of the remote sensing system. Wrapping fiber around the pipe can provide the best spatial resolution and sensitivity to the pipe vibration, but significantly increases the installation cost and shortens the sensing range. Clamping or taping a straight fiber outside the pipe are more practical options, but can still be expensive or impossible for buried pipelines. Deploying a sensing cable inside the pipeline can be much cheaper and easier compared to external cable deployment, as the cable can either be pumped down or dragged along by a tractor device. However, cable inside the pipeline can be directly affected by the flow, which imposes challenges on sensing the pipeline vibration directly. Meanwhile, different cable structural designs also affect the sensing results.

1.2. Objectives in the 3rd Annual Report Period

In this project, we plan to solve and answer several fundamental but practical questions for using DAS to assess pipeline integrity risks, which include:

- The feasibility of using DAS to identify vibrations that are associated with pipeline integrity risks, which include liquid accumulation at lower spots, slug flow, internal corrosion, dent, damaged infrastructure, and leakage.

- The effectiveness of sensing the aforementioned vibrations using different sensing cable deployment methods, especially for cables inside the pipeline.

2. Experimental Program in the 3rd Annual Report Period

2.1. Experimental Design

To achieve the research goal, we perform the experimental study at Edgar Mine, an experimental mine of Colorado School of Mines (CSM) located approximately 20 miles west of Denver. The location and picture of the experimental facility are shown in Figure 1. The flow loop is inside the tunnel, which has a constant environment that eliminates measurement uncertainties. The mine is relatively dry and has a constant year-round temperature of 54°F. The mine is well-equipped with utility systems that allow the operation of equipment for maintenance and experimentation.

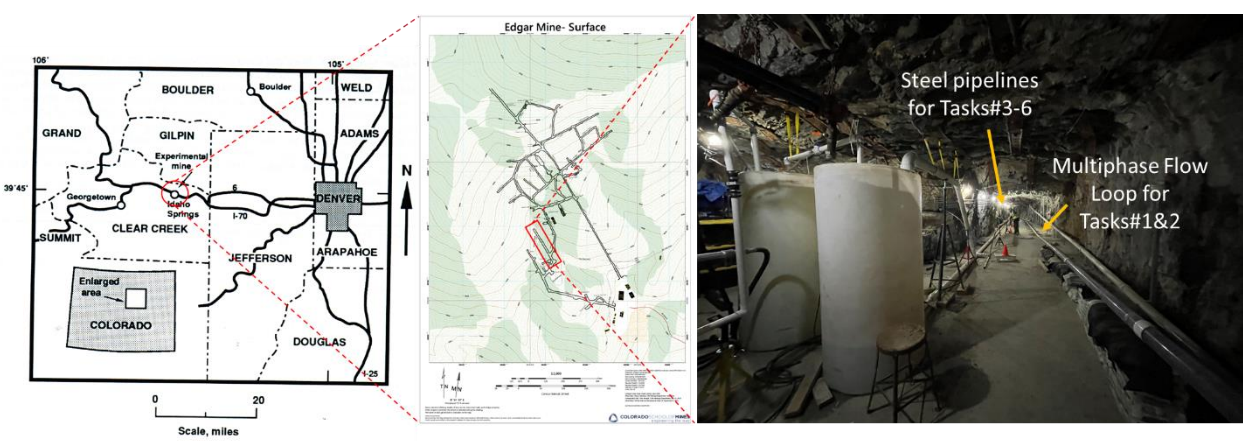

Figure 1. Testing facility for this project at Edgar Mine.

Tasks#1 and #2

The experimental setup for Task#1, targeting for the Detection of Liquid Accumulation at Pipeline Lower Spots, and Task#2, focused on the Detection of Dynamic Intermittent (Slug) Structures, was implemented using a transparent PVC pipeline flow loop. This setup facilitated direct visualization of flow patterns, which could then be correlated with DAS measurements.

To simulate a low spot for water accumulation, a custom PVC pipe was constructed with specific inclines. The low spot was positioned 42 feet from the start of the loop, followed by a section with a 2-degree upward slope. The overall length of the experimental segment, which included the clear PVC portion, spanned 150 feet.

Externally, a single-mode jacket cable was helically wound around the PVC pipes, using 100 feet of cable for every 10 feet of pipe, with a wrap spacing of 3 cm. The cable was held in place using tension and duct tape. Inside the PVC pipe, three types of cables (thin, thick, and flat) were freely deployed. These internal cables exited through custom seals at both ends of the clear section. Figure 2 provides a schematic of the multiphase flow loop. Figure 3 shows the pictures of the testing facility and a closer look of some specific parts, as well as the connections of the fiber optic cables. Two pressure sensors were installed. One sensor was placed at the inlet, downstream and downhill from the start, while the second sensor was positioned in the middle of the uphill section. Both pressure sensors were interfaced with a LabView Data Acquisition system, as were the control valves responsible for regulating the air and water inlets. The operational data, including the pressure and flow rates, were recorded at a frequency of 10Hz.

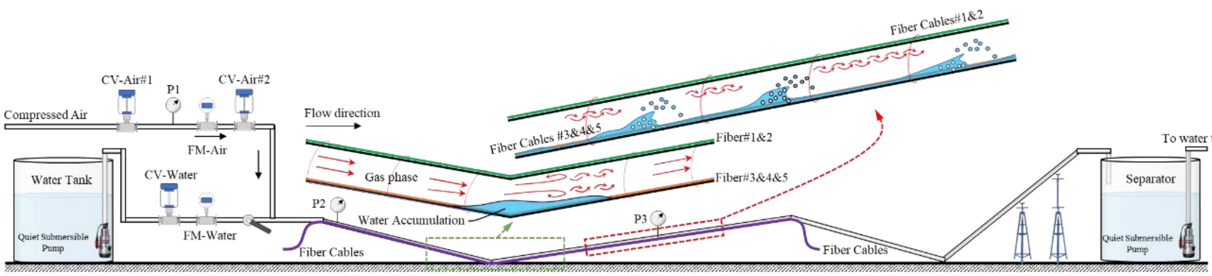

Figure 2. Schematic of testing facility for Tasks#1 and #2.

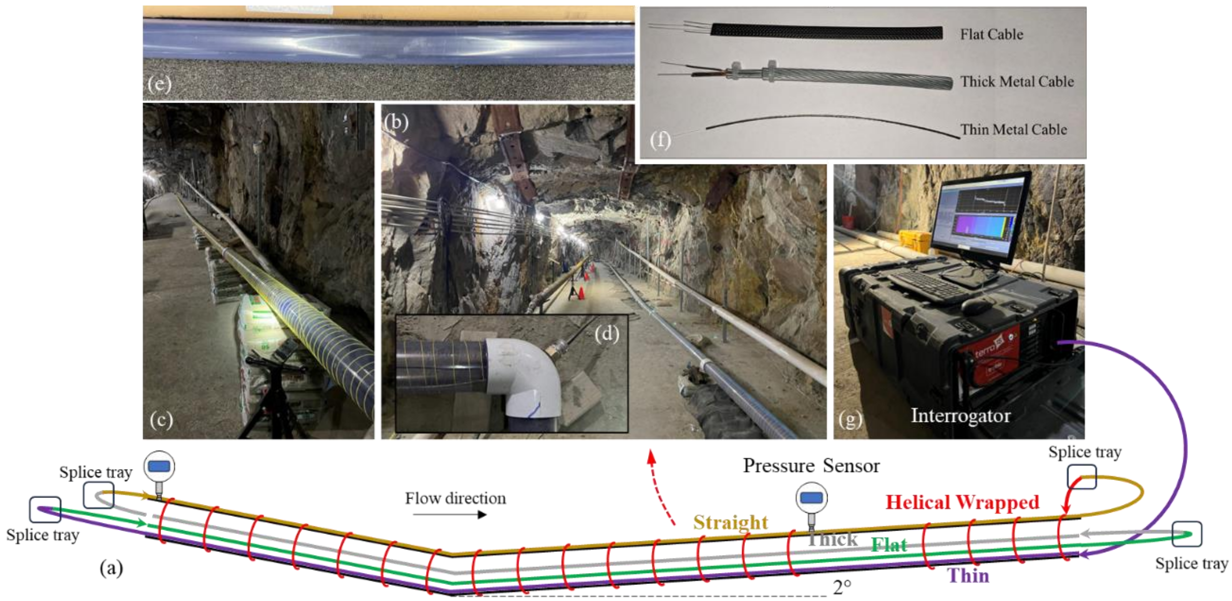

Figure 3. (a) Schematic showing the connection of different fiber-optic cables using splice trays, with the thin cable connected directly to the interrogator unit; (b) Picture of the multiphase flow loop and the test section; (c) Closer picture of the test section; (d) Picture of the seal for internal cables; (e) Picture of the V-section; (f) Picture of the three internal deployed cables (flat, thick, and thin from top to bottom); (g) Picture of the interrogator.

Tasks#3 to #6

Densely and sparsely supported pipeline: To investigate Tasks #3-6 in a controlled environment, we constructed a steel pipeline at the Edgar Mine experimental facility. Figure 4 illustrates the steel pipeline, which is situated inside the tunnel, which provides a quiet environment, eliminating measurement uncertainties and minimizing ambient noise contamination. We used an industry-standard pipe, carbon steel seamless API 5L Grade X65, with a 4-inch internal diameter. The pipeline measures 21 meters in length and features a 1-meter section in the middle that can be modified to adapt to various experiments. The entire steel pipeline is connected to the main air supply from the Mine air compressor using a flexible hydraulic hose, and is supported with tripods. The number of tripods in place is changed accordingly to test the different configurations proposed for the project densely and sparsely supported pipelines.

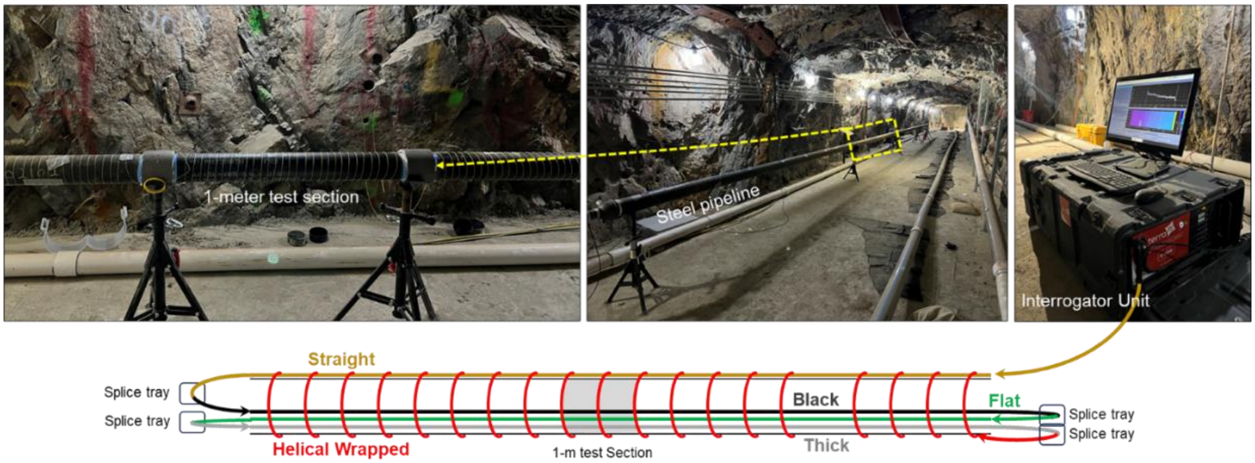

Figure 4. Middle: Photograph of the steel pipeline; Left: Photograph of the 1-m section in the middle of the steel pipeline; Right: Picture of the interrogator unit; Bottom: Schematic showing the fiber connections.

One of the objectives of this project is to compare the sensitivity and detectability of different fiber optic cables. To achieve this, we equipped the steel pipe with various types of single-mode optical fiber cables, with the pictures shown in Figure 5. Three cables are deployed internally: a black cable, a flat cable, and a thick cable that closely resembles a wireline cable. The black and flat cables are standard outdoor distribution fiber cables. The steel pipe was also equipped with external yellow jacket cables: a straight, and a helically wrapped spaced at 3 cm intervals, as illustrated in Figure 4. However, the wrapped cable was excluded from the study because it frequently experienced breakages, which compromised the data quality and made it impractical for consistent use. This highlights that the yellow jacket fiber may not be suitable for field deployment, as it is easily susceptible to breakage. The internal cables are introduced into the pipeline through a specially designed rubber-sealed fitting at the inlet, which maintains the pipeline pressure. This fitting is assembled flexibly to facilitate the easy movement of the internal cables, allowing for the convenient replacement of the 1-meter test section in the middle of the pipeline based on the experiment being conducted. The internal cables are free-floating and not intentionally secured to the pipe wall. The cables are connected in the following order: straight linearly taped, black, flat, and thick (see Figure 4). Splicing of the cables was performed at opposing ends of the pipeline test section using splicing trays. When all five cable deployments were linked together, they formed a combined fiber length of approximately 220 meters. The cables are connected to the Terra15 interrogator that enables DAS data acquisition.

Figure 5. Photographs of the tested fiber optic cables

As detailed in the Year 2 Annual Report, the core experimental framework (test matrix) remains consistent across Tasks #3-6, primarily involving the flow of single-phase air at standard velocities of approximately 2 m/s, 6 m/s, 10 m/s, 14 m/s, and 18 m/s. For this reporting period, we added a cap at the pipe outlet, in order to study the cable detectability at different background pressures ranging from around 1 to 10 psi. For some tasks, we conducted tests with different valve settings (fully open, half open, and fully closed) while maintaining a constant flow rate. The maximum flow velocity tested was 11 m/s, the highest achievable under safe conditions, to generate the maximum possible pipe pressure, thereby improving the cables' ability to detect damage in the 1-meter test section. Additionally, a pressure sensor was installed at the beginning of the steel pipe to monitor in-situ pipeline pressure.

The key variation between the different tasks lies in the customization of the central 1-meter pipe to correspond with the specific studied task, as follows:

Task#3: In this task, the central pipe incorporates a 1-m test section with varying levels of corrosion, simulating three scenarios: one representing minimum corrosion with a depth of 3 mm, the second referring to moderate corrosion with a depth of 5 mm approximately, and the third referring to severe corrosion with minor leakage (~2 mm in diameter) which is shown in Figure 6. The procedures for inducing corrosion on the internal pipe surfaces and achieving the desired corrosion depths are thoroughly described in our previously submitted Year 2 Annual Report.

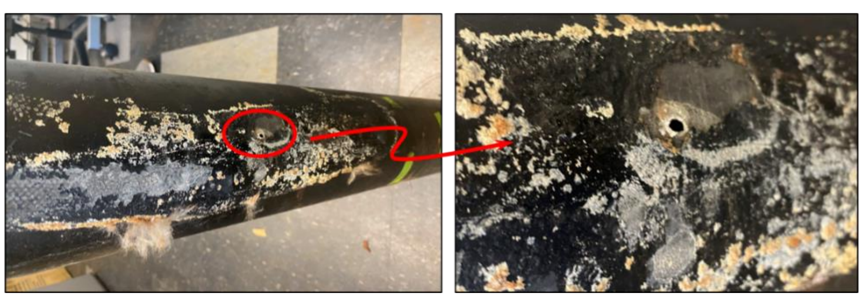

Figure 6. Photograph of the 1-m corroded pipe with minor leakage (~2mm) at pipe bottom.

Task#4: This task involves replacing the 1-meter test section with a deformed pipe to simulate dented pipelines commonly encountered in field conditions. Two different dent sizes were tested using two distinct dented pipes. One pipe exhibited substantial deformation, representing a significant structural compromise, while the other displayed a smaller dent, simulating a less severe scenario (Figure 7 and Figure 8).

Figure 7. Photograph of the facility that created the dents and the 1-m test sections with two dent sizes.

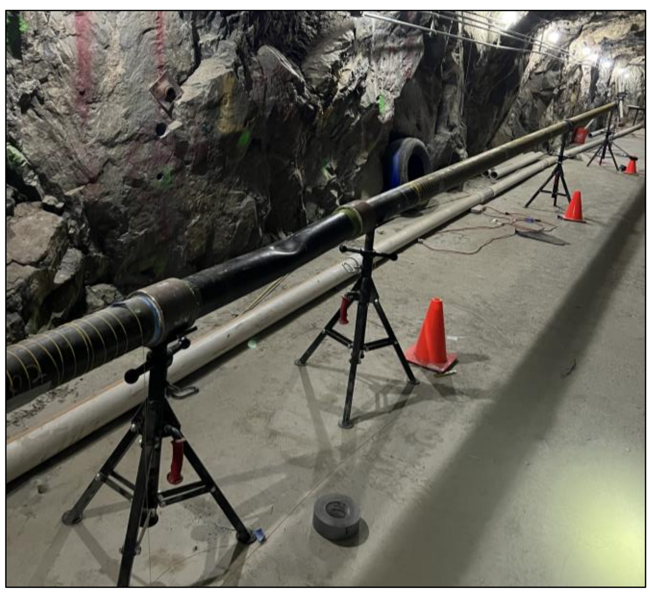

Figure 8. Photograph of the 1-m pipe with large dent positioned at the center of the steel pipe.

<u>Task#5</u>: In this task, we investigate infrastructure damage detection with the central 1-meter section remaining intact and free of defects. The only modification involves varying

the number of tripods supporting the entire pipeline. In the previously reported findings (refer to the Year 2 Annual Report), we tested a base case for a sparsely supported pipeline, where 5 supports were evenly distributed along the 21-meter steel pipeline. To simulate support damage, the second support from the inlet was removed, resulting in a total of 4 supports for the damaged condition. For the densely supported pipeline, 6 supports were used in the base case, and similarly, the second support from the inlet was removed to simulate damage. For this reporting period, we tested a different configuration where 5 supports were initially evenly distributed along the pipeline. We then removed the support located at the center of the pipeline, which corresponds to the middle of the 1-meter test section.

<u>Task#6</u>: It involves a 1-m test section with 1" holes at three different positions (top, side, and bottom), enabling the simulation of leakage at various orientations. Combined with reducers with three different sizes (Figure 9d), we can simulate four leakage sizes, namely ¼", ½", ¾", and 1". Additionally, a pressure sensor is incorporated to record central pipe pressure during experiments. The removable cap installed at the pipe outlet helped increase the pressure differential between the pipe and atmospheric conditions at the leakage points, enhancing data quality and DAS detectability.

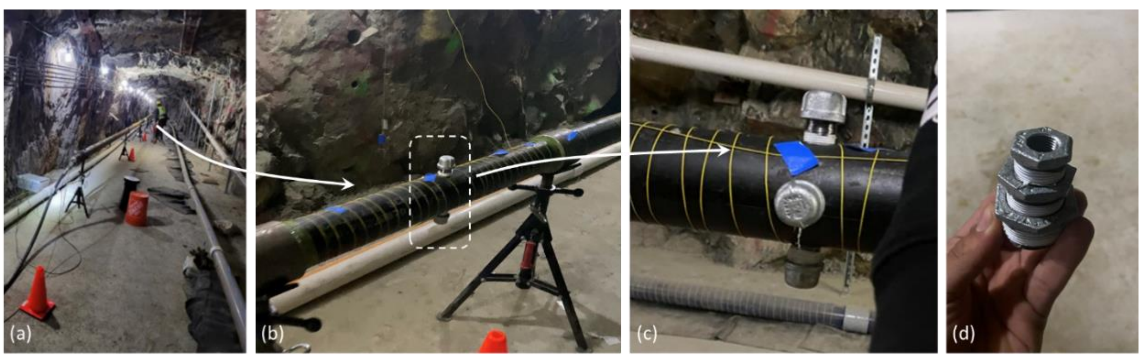

Figure 9. (a) A picture of the facility; (b) 1-m test section for leakage detection; (c) holes with caps on the 1-m test section; (d) reducers for hole size control.

<u>Buried and Unburied Pipeline</u>: During the current reporting period, we modified the facility for testing different pipeline defects in unburied and buried configurations (Figure 10). To achieve this, wooden boxes were ordered and subsequently modified on-site to secure the pipes. The wooden boxes were partially filled with sand before placing the pipe on top, with additional sand added around the sides to ensure the pipe remained stable and secure, minimizing vibrations. The pipe is now securely positioned on the sand. We anticipate observing different vibration patterns during data analysis compared with supported configurations. To prevent sand from being displaced during Task#6 experiments (leakage detection), a tarp was placed underneath the leakage point, as shown in Figure 10. In the unburied setup, the pipe rests on top of the sand. After testing in the unburied configuration, the pipe will be buried under the sand to simulate the buried pipe condition.

Before transitioning the pipeline to its ground-laying configuration, we made a strategic decision to repeat most of our experiments. This decision was based on the understanding that once the pipeline was laid on the ground, it would be difficult to revert it back to its previous supported setup. To ensure that our findings are repeatable and robust, we conducted the experiments again in the initial configuration.

Figure 10. (a, b) Photograph showing the unburied pipe installation; (b) Picture of the 1-m test section.

2.2. Test Procedure

- <u>Laboratory Testing:</u>

  For Task #1, the experimental procedures involved varying the volumes of stagnant water accumulation, specifically 4L, 10L, and 20L, while testing at flow velocities of approximately 2 m/s, 4 m/s, and 6 m/s. The air flow valve was adjusted to achieve these target velocities, which were maintained for at least 10 minutes to ensure that fully developed flow conditions were reached.

  For Task #2, aimed at detecting dynamic intermittent (slug) structures, a combination of air and water was introduced into the PVC flow loop. The water valve was kept constant to maintain a steady flow rate, while adjustments to the air valve were made to achieve the desired velocities: 18 m/s, 16 m/s, 14 m/s, 12 m/s, 10 m/s, 8 m/s, 6 m/s, 4 m/s, and 2 m/s. Single-phase experiments were also performed at these same velocities to establish a baseline for comparison with the multiphase flow results.

  For Task#3, please refer to the 1st and 2nd annual reports for details on the procedures and methods to induce corrosion to the 1-m test sections.

  The previous section details the tests for Tasks#3 to #6.

- Field Testing:

  None.

3. Results and Discussions

3.1. Task#1: Detection of Liquid Accumulation at Pipeline Lower Spots

The results obtained from experiments involving water volumes of 4L, 10L, and 20L at velocities of 2 m/s, 4 m/s, and 6 m/s, as recorded by DAS data, reveal promising capabilities in the detection of liquid accumulation within pipeline low points. Figure 11 shows the processed DAS data recorded with around 4 m/s gas velocity with the three different water volumes. A clear low-frequency vibration can be observed by the flat cable near the V section, which is associated with wavy liquid surface and water-cable interaction.

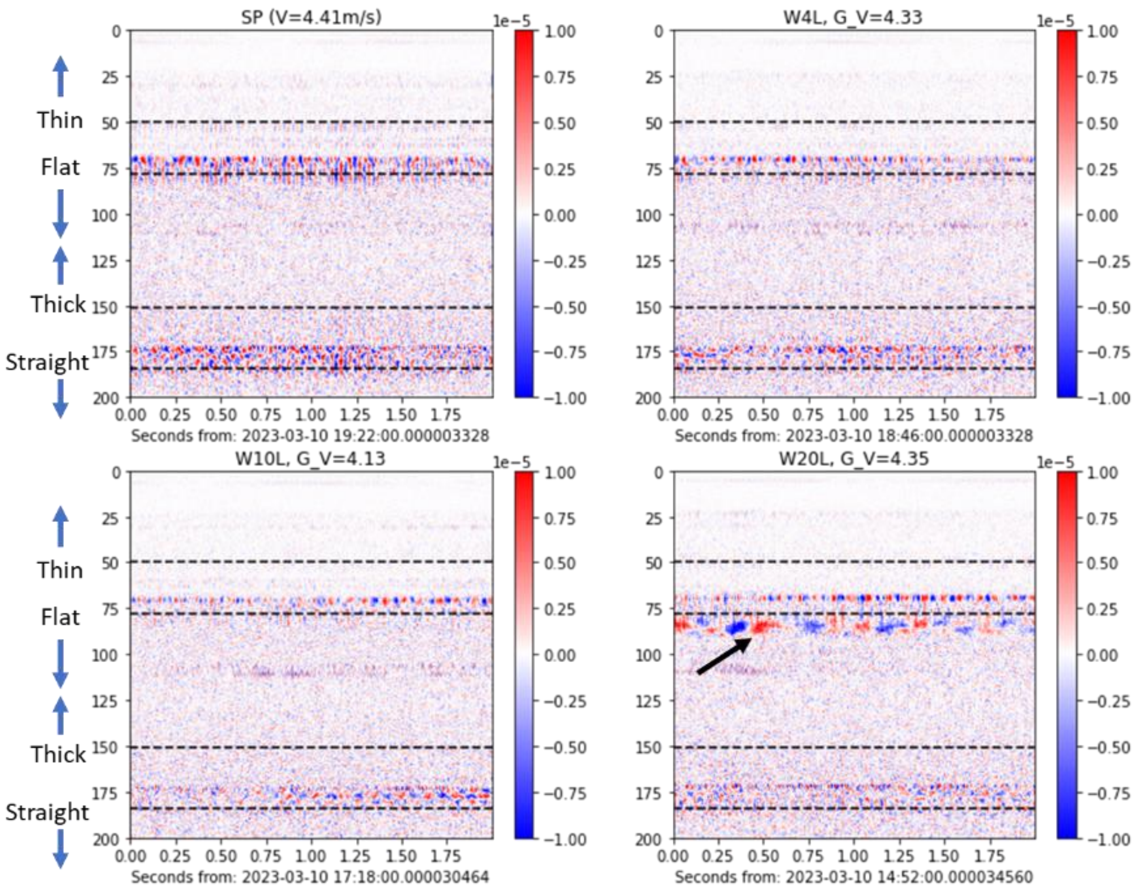

Figure 11. Waterfall plots for DAS raw data all observed at around 4 m/s gas velocity with different volumes of water accumulated at the V-section. The vertical axis is distance along the fiber in meter, and horizontal axis is time. Top row: no water accumulation (left), 4L water accumulation (right). Bottom row: 10L water accumulation (left), 20L water accumulation (right). The location of V-section is indicated by black dashed lines. From top to bottom, the dashed lines mark the V-section location for thin, flat, thick, and straight cables. Blue arrows

indicate flow direction in each fiber section. Black arrow highlights the vibration of flat cable associated with the wavy liquid surface.

In further data analysis, each channel's spectrum was computed on a per-second basis, facilitating spectrum analysis with a specific emphasis on the V-section across various cable designs. This analytical approach produced a spectrum curve for each cable design at different water levels, as illustrated in Figure 12. Across all cable designs, a distinctive peak consistently emerged at a frequency of 20 Hz, aligning with scenarios of no water volume presence. However, as the volume of water increased, this 20 Hz peak gradually diminished, reflecting the dampening effect of water on vibration patterns.

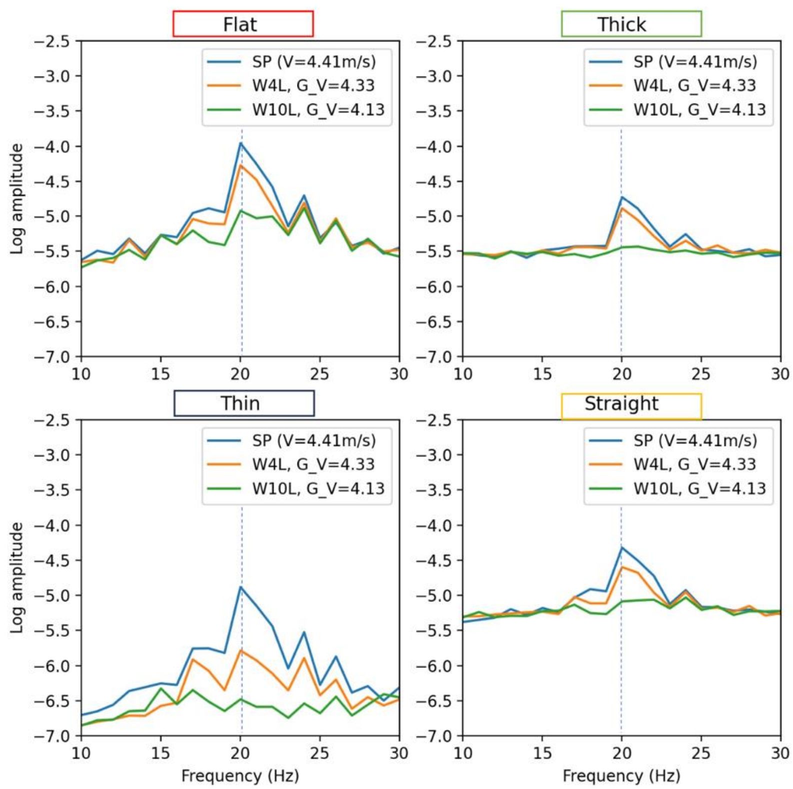

Figure 12. Frequency spectrum of DAS measurements near the V section for various cables at a gas velocity of approximately 4 m/s. SP (single phase) denotes conditions with no water accumulation. W4L, W10L, and W20L correspond to 4L, 10L, and 20L of accumulated water, respectively. Amplitudes are presented in a logarithmic scale. The prominent peak around 20 Hz is distinctly indicative of the accumulated water volume.

Furthermore, our analysis involved the computation of standard deviation values for each second within every channel of the DAS data, shown in Figure 13. By visualizing the data in this manner, we observed the onset of slug-like behavior at a velocity of 4 m/s with a water volume of 20L. The spectrum curve for 20L did not show similar trends to those of 10L, 4L and 0L (single phase), as shown in Figure 12. This deviation in the 20L data can be attributed to the emergence of slug behavior, a phenomenon not observed at lower water volumes. Consequently, this behavior departs from the trends observed at 20 Hz.

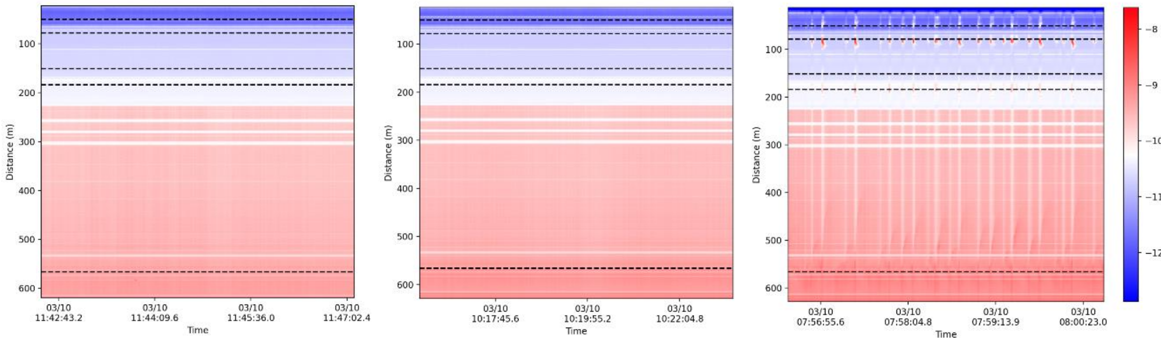

Figure 13. Standard deviation plots for 4L (left), 10L (middle), and 20L (right) water accumulation tests. Slugging start to appear when the liquid volume is above 20L, which are indicated by the high amplitude signals in the SD plots. No slugging behavior was observed for 4L or 10L tests. The superficial gas velocity is 4 m/s.

3.2. Task#2: Detection of Dynamic Intermittent (Slug) Structure

The experimental investigation of multiphase flow, with water flow rates of 0.3 and 0.6 GPM (0.0025 and 0.005 m/s) and air flow rates varying between 18 m/s and 2 m/s, demonstrated the effectiveness of DAS in capturing dynamic slug structures. A comparison between raw and processed DAS data, and its correlation with pressure sensor readings, confirmed the system's sensitivity to slug detection.

Different data processing algorithms were utilized to characterize the dynamic slug flow behaviors, including various filters, standard deviation, and specific designed algorithms for slug frequency and velocity determination.

From the data analysis, we have seen that all the cables captured the slugging behavior well. It also captures the slugging initiation and dissipation processes well.

Building upon these observations, a dedicated slug detection algorithm was implemented to identify and analyze slugs detected at each DAS channel along the pipeline's length. The slug frequency distribution along the pipeline testing section illustrates the dynamic and intermittent nature of slugging behavior. A notable increase in slug frequency is observed near the low spot at 50 meters, particularly at a velocity of 2 m/s. This increase corresponds to the low spot point in the pipeline which promotes slug formation due to the liquid accumulation at low gas flow rate conditions. The slug frequency stabilized at around 10-15 meters away from the low spot in the uphill section. The amplitude of the SD DAS data generally increases as it moves away from the low spot, indicating that only stronger slugs can sustain over long distances. Interestingly, the decrease in slug frequency generally coincides with an increase in the amplitude, indicating slug decay and growth as explained previously. On the other hand, the deviation shows that, while the new slugs forming at the low spot are small, they exhibit less divergence compared to those far downstream in the uphill section.

In contrast, the helically wrapped cable, with its superior spatial resolution, provided more complete insights, as shown in Figure 14. The slug initiation and dissipation processes are clearly illustrated in the DAS signals. The slugs may undergo several changes while they travel along the pipes, especially for the small ones. An example of this can be seen with the first slug in Figure 14. This slug forms near the inlet of the uphill section, and gradually decays as it climbs up the uphill section, after several reformation and dissipation processes. This type of slug is normally smaller in size, contains less liquid volume in the slug body, and travels at lower speeds. On the other hand, the strong slugs, which are normally large and have more liquid volume in the slug body, can sustain over a longer distance, generating stronger responses in DAS signals (see the last slug shown in Figure 14). We anticipate that, the absolute value of the DAS amplitude in the waterfall plot, which is in the unit of strain rate, should correspond to the slug size (or the liquid volume in the slug body), which is related to its velocity. The data reveal that the more pronounced slugs – characterized by their greater amplitudes – tend to travel at higher velocities.

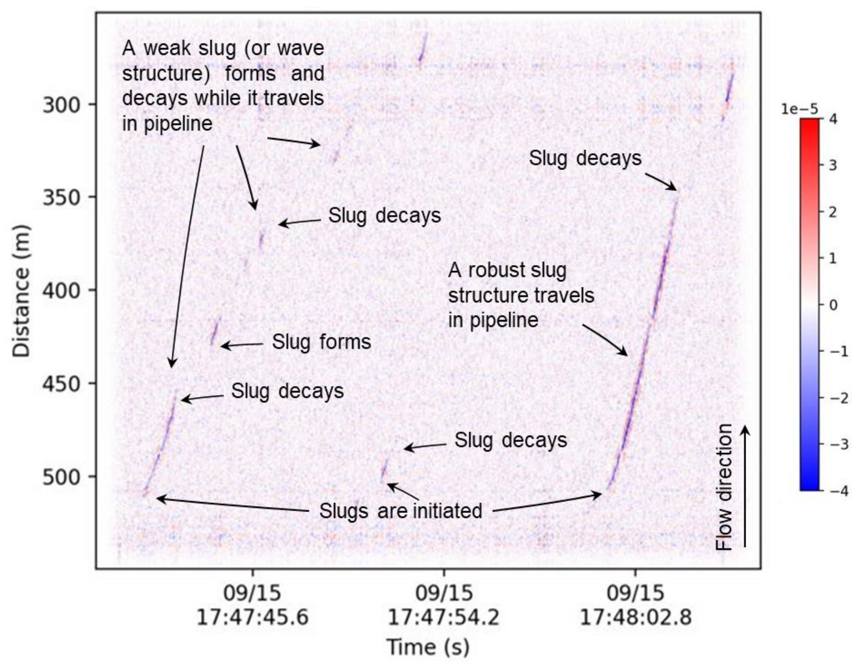

Figure 14. Processed DAS data in a 40-second temporal window captured by the helically wrapped cable. The data illustrates cycles of slug formation and dissipation, culminating in the emergence of a pronounced slug structure towards the end of the window, exhibiting higher velocity.

The sensitivity of different deployed cables is illustrated in Figure 15, that shows the standard deviation processed DAS data for the four linearly deployed cables, including the three internal cables (thin, flat, and thick) and the external straight cable. The comparison highlighted the heightened sensitivity of the flat cable to slug detection, possibly due to the flat shape that can be influenced by the fluid flow behavior more easily. Conversely, the internal thin cable and the external straight cable yielded more qualitative results in slug characterization. While the flat cable exhibited a heightened amplitude response to slugs, the sensitivity seems to vary along the cable, generating discontinuities within individual slug signals. Meanwhile, the delineation of slug patterns was more pronounced in the thin and straight cables, revealing a clearer sloping trend that is good for velocity determination. The thick cable, however, provided the least sensitivity among all, which could be due to the rigid metal structure that weakened the fiber and fluid flow coupling.

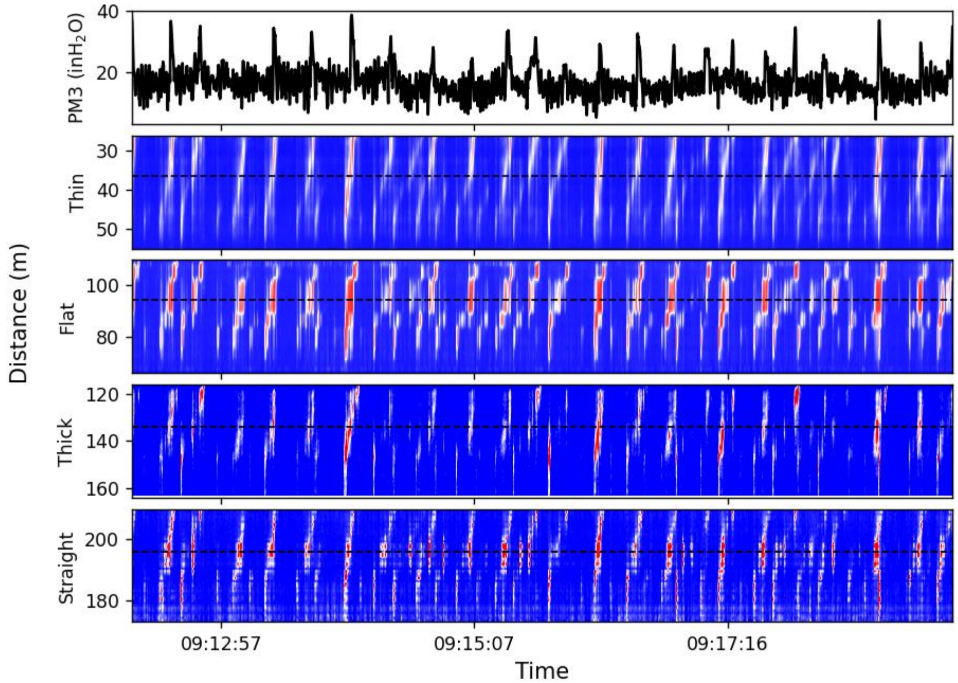

Figure 15. Visualization SD-processed DAS data overlaid with pressure sensor readings for the thin, flat, thick, and straight cable sections. The black dashed lines indicate the locations of pressure sensors within each cable section. The observed slugging behavior is depicted as subtle, sloping trends. Clearer delineation of slug behavior is evident in the thin and straight cable compared to the flat cable, while the thick cable exhibit poorer sensitivity to slug passage. The data corresponds to superficial gas velocities of 4 m/s at a liquid flow rate of 0.6 GPM.

3.3. Task#3: Detection of Corroded Spots on Pipeline Interior Surface

During this reporting period, we finalized the preparation and testing of the three corroded pipes: the 3 mm corroded pipe, the 5 mm corroded pipe, and the severely corroded pipe with a minor leakage for supported pipeline configuration. Our initial experiments focused on the severely corroded pipe with minor leakage, where we conducted tests at five different standard flow velocities (2, 6, 10, 14, and 18 m/s). However, based on insights gained from Task#6 (Leakage Detection), we implemented additional tests to enhance the detectability of the minor leakage located at the bottom of the severely corroded pipe. As detailed in the experimental design section, a pressure sensor was installed at the beginning of the steel pipe to continuously monitor in-situ pipeline pressure. We then performed a series of tests with different manual valve openings at the steel pipe's end (fully open, half open, and fully closed) while maintaining a constant in-situ flow rate in the pipeline. The maximum achievable flow velocity under safe conditions was 11 m/s, which we aimed to achieve to generate the highest possible differential pressure across the leakage, thereby improving the detectability of the minor leakage by the cables.

For data processing we first analyzed the standard deviation data to investigate the detection of the minor leakage at the bottom of the corroded pipe. Initially, the calculated STD data did not clearly reveal the leakage. However, after optimizing the display parameters and scale, we improved the detection of the minor leakage (see Figure 16 and Figure 17). Particularly, the black, and flat cables exhibited detectability, especially when the valve at the end of the steel pipeline was closed. This configuration increases differential pressure across the leakage, helping in leakage detection. Figure 16 and Figure 17 also indicate that an increased pressure difference improves the cables' ability to detect the leakage. In these figures, the leakage is positioned near the middle of the cable section and indicated by the black transparent dashed lines at each waterfall plot. Given that the operating pressures in actual field conditions are significantly higher than those in our tests, we are optimistic about the black cable's potential to identify and detect minor leakage spots in the field more effectively. Notably, the black cable exhibited the highest sensitivity to the minor leakage present at the bottom of the corroded pipe.

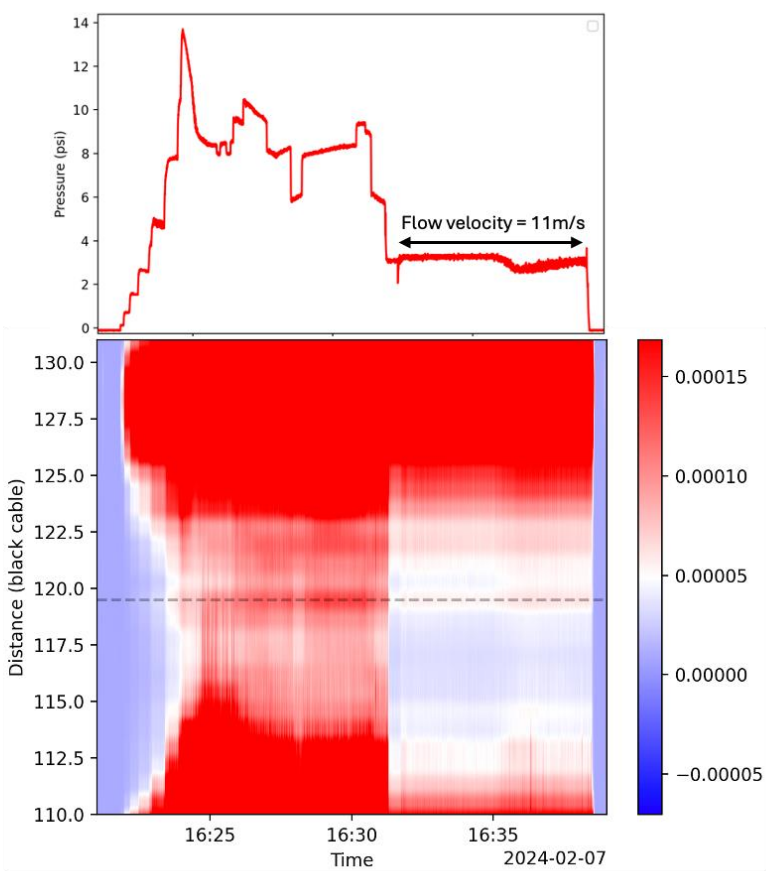

Figure 16. Top: the pressure within the pipeline; bottom: the DAS standard deviation data along the black cable. Flow direction is from bottom to top. The location of the leakage is marked by a dashed, black transparent line. The valve at the end of the pipeline is closed. Note that, from around 16:22 to 16:32, we tried to adjust the inlet gas valve to achieve the desired velocity 11m/s, which was achieved at around 16:32. We showed the data in this entire period, because it shows interestingly how the DAS signal corresponds to the pressure and/or flow rate changes. It also shows that the higher differential pressure across the leakage point, the better its detectability using fiber cables.

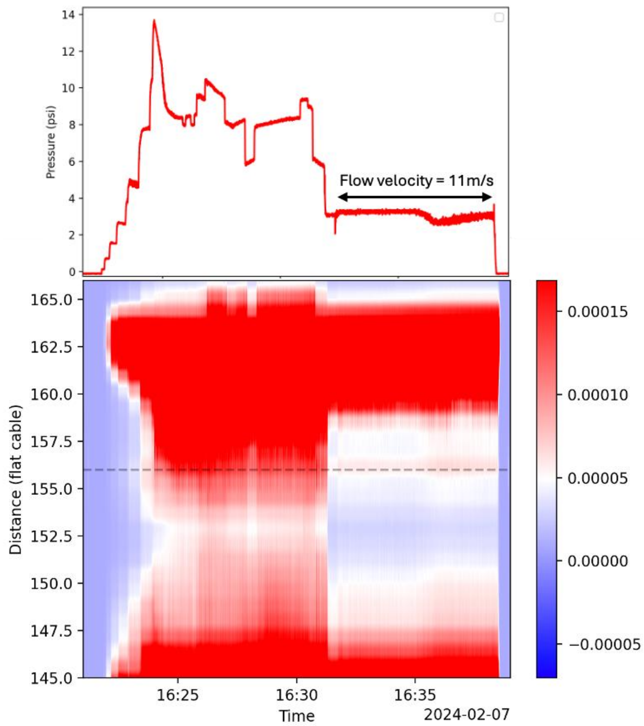

Figure 17. DAS data with adjusted scale that shows more clearly on the leakage.

We repeated the experiments for the severely corroded pipe using two pipe installation methods: one initially supported by five supports and then with the middle support removed. The data was analyzed and compared to the control experiments conducted on a 1-meter pipe with no defects under the same two configurations (five supports and four supports). The findings confirmed the previous observations.

We also repeated the experiments for the 3 mm corroded pipe and completed testing on the 5 mm corroded pipe. However, the current data could hardly see these corrosions. In the future, we will explore more deeply using different data processing algorithms to investigate the cable detectability on these corroded pipes.

During this reporting period, we also conducted the corrosion experiments using the severely corroded 1-meter test section with a tiny leak (2~3 mm) at the pipe bottom, with the unburied pipeline configuration. Preliminary data analysis showed promising results.

3.4. Task#4: Detection of Dent/Deformation on Pipeline

During this reporting period, we completed the testing of two dented pipes. One pipe showcased a substantial deformation, simulating a significant structural compromise, while the other presented a smaller dent, simulating a less severe scenario (Figure 7). We conducted experiments on both pipes, testing five different flow rates (2, 6, 10, 14, 18 m/s). The resulting data is compared to experiments conducted on the central 1-m section of the pipe without defects, serving as our baseline or control experiment in the data processing workflow section.

The data analysis shows promising results for DAS in detecting the dents. Moving forward, our upcoming efforts will focus on conducting additional analysis and refining our workflow to delve deeper into comprehending the underlying physics behind our findings and ensuring their reliability.

3.5. Task#5: Detection of Infrastructure Damage

In this task, part of the infrastructure damage investigation, we utilized an intact and defect-free central 1-meter section of the pipeline. The primary modification involved varying the number of tripods supporting the pipeline. In contrast to previous tests, we initially used five evenly distributed supports along the pipeline and then removed the support located at the center, corresponding to the middle of the 1-meter test section, to simulate support damage. The data analysis shows promising results for DAS in detecting these changes.

3.6. Task#6: Detection of Leakage

In this reporting period, we repeated some leakage experiments to enhance the reliability of our findings. We successfully reproduced the results reported in our submitted Year 2 Annual Report and improved upon some of them. Same as reported previously, the leakage tests involved a 1-m test section featuring 1" holes positioned at three different orientations to simulate various leakage scenarios. Through the use of reducers, we were able to test four different leakage sizes: ¼", ½", ¾", and 1". Additionally, we conducted tests using five gas flow rates: 2, 6, 10, 14, and 18 m/s. Prior to each leakage experiment, a control experiment (without any leakage) was conducted to ensure a more consistent basis for comparison.

In this section, we will briefly review the data processing workflow outlined in our previous annual report, which we have consistently applied to process the data collected during this reporting period. The DAS data acquisition was performed with a temporal sampling frequency of 14.39 kHz and a spatial sampling rate of 0.82 meters along a 220-meter fiber, generating a substantial volume of data in a short period. For instance, the three-hour recording session yielded over 150 GB of DAS data. Due to its size, this data set requires pre-processing before any meaningful analysis can be conducted. The first processing we conducted was based on the standard deviation (SD). We segment the data set into one-second intervals and compute the SD for each channel within each second. These SD values are then concatenated into a continuous data set with a 1 Hz sampling rate. This method allows for a data reduction factor of 14,390, equivalent to the original sampling rate. Figure 18 provides an illustrative example of the STD data attributes during an experiment involving bottom leakage holes. In this figure, a higher value (depicted in red) signifies a larger standard deviation at a specific time and location along the sensing fiber, which in turn is indicative of higher vibration intensity experienced by the cable section.

The figure displays the vibration intensity for four distinct types of cables during the experiment conducted on the same day. The study commenced with a control experiment featuring no leakage, followed by the sequential introduction of 1", ¾", ½", and ¼" leakage holes at the bottom of the test pipe. For each hole size, flow rates of 2, 6, 10, 14, and 18 m/s were examined. Figure 18 clearly reveals variations in fiber vibration intensity at different flow rates, with higher flow rates inducing stronger vibrations across all cable types.

Notably, more intense vibrations are visible near the pipe's center, where the leakage was introduced, for straight, black, and flat cables. The vibration anomaly appears to diminish with decreasing hole size and is entirely absent in the control tests. Unlike the experimental setup detailed in the previous quarterly report, this time, the straight cable was secured to the pipe using duct tape, significantly improving the mechanical coupling of the fiber. This enhancement notably increased the cable's detectability, this can be seen clearly from the standard deviation data.

To quantify the vibration anomalies associated with the leakage points, we calculated the average vibration intensity over a four-minute span in the middle of each experiment. This average intensity forms a vibration profile for each cable, and the amplitude is then converted to decibels (dB) for easier comparison. Figure 19 illustrates the sensitivity of various cables to different leakage sizes, particularly at a flow rate of 10 m/s. The thick cable, being notably heavier, shows the least sensitivity to vibrations induced by the leakage. However, the other three cable types demonstrate varying degrees of sensitivity to detect the vibration anomaly caused by different leakage sizes. It's noteworthy that improving the mechanical coupling of the straight cable significantly contributed to enhancing its ability to detect the vibration anomaly caused by leakage, as depicted in Figure 19.

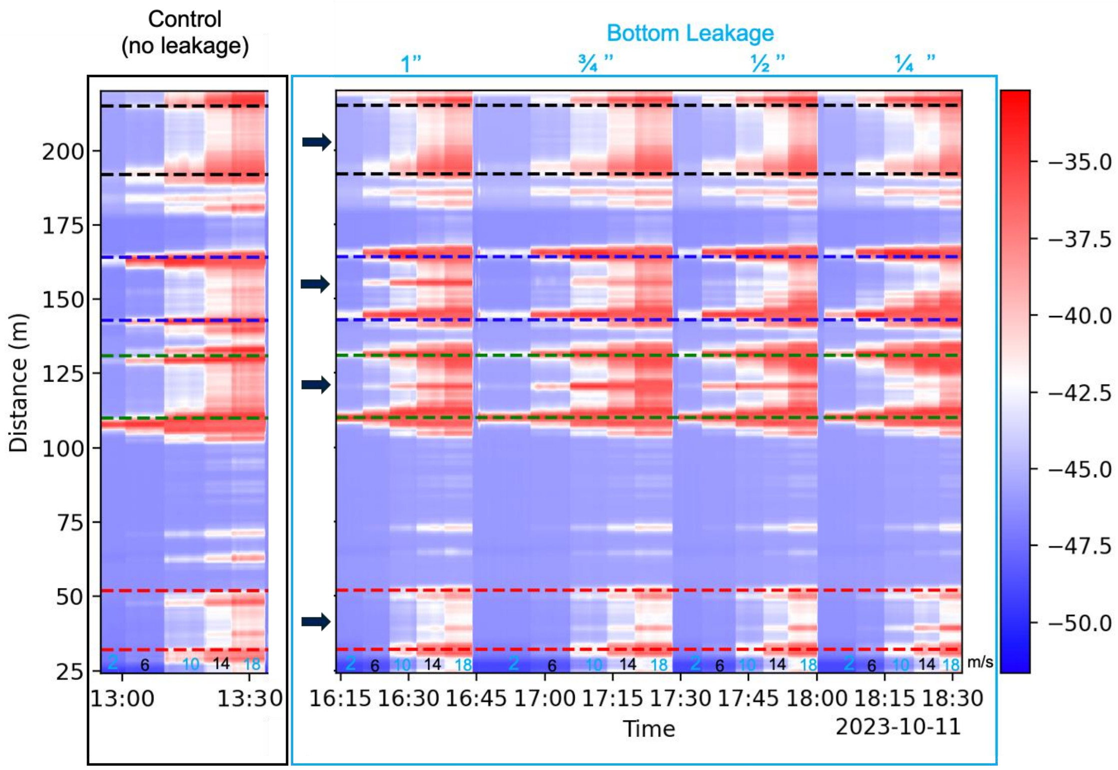

Figure 18. Magnitude of standard deviation values in straight external (red), black (green), flat (blue), and thick (black) fiber sections during the control, and bottom leakage experiments with different hole sizes. The flow velocities inside the pipe change from 2, 6, 10, 14 and 18 m/s (The gas velocities are indicated at the bottom of the figure). The arrows indicate the leakage location (at the center of all cable sections).

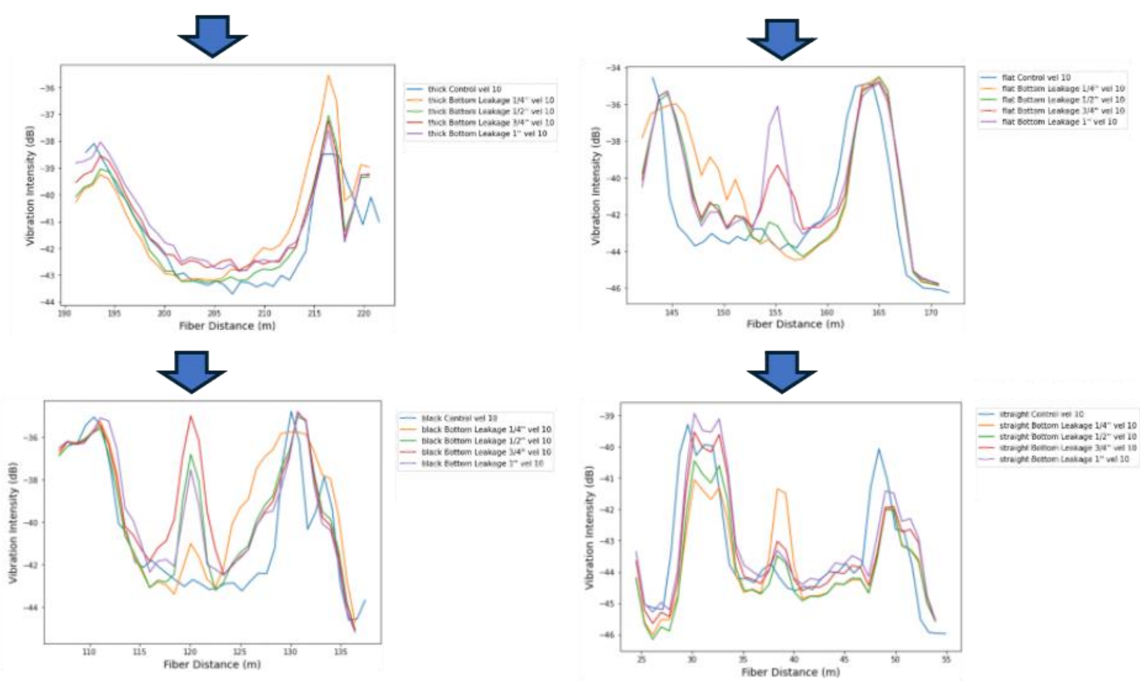

Figure 19. vibration intensity profiles in thick (upper left), flat (upper right), black (bottom left), and straight (bottom right) fiber sections during the leakage experiment. The different curves represent vibration intensities associated with varying leakage hole sizes at a flow rate of 10 m/s. Anomalies in vibration, induced by leakage holes and marked by blue arrows, are observable in three cable types when the hole size exceeds 1/2 inch.

Leakage detection sensitivity is also influenced by the gas flow rate within the pipe. Figure 20 illustrates the vibration distribution along the four fiber cables at different flow rates. For instance, in the control experiment, vibration intensity escalates with increasing flow rates for the flat cable, and no vibration anomaly is observable at the pipe's center. Conversely, in the experiment with a ½" leakage hole, a vibration anomaly is observable at all flow rates for straight, flat, and black cables, while the thick cable shows no such response. Our findings indicate that black and flat internal cables provide the most reliable leakage detection results observed thus far. Their lighter and more flexible structures likely increase their sensitivity to fluid movements within the pipe. Furthermore, it's worth noting the validation of our hypothesis: improving the mechanical coupling between the external cable and the steel pipe notably enhanced its detectability.

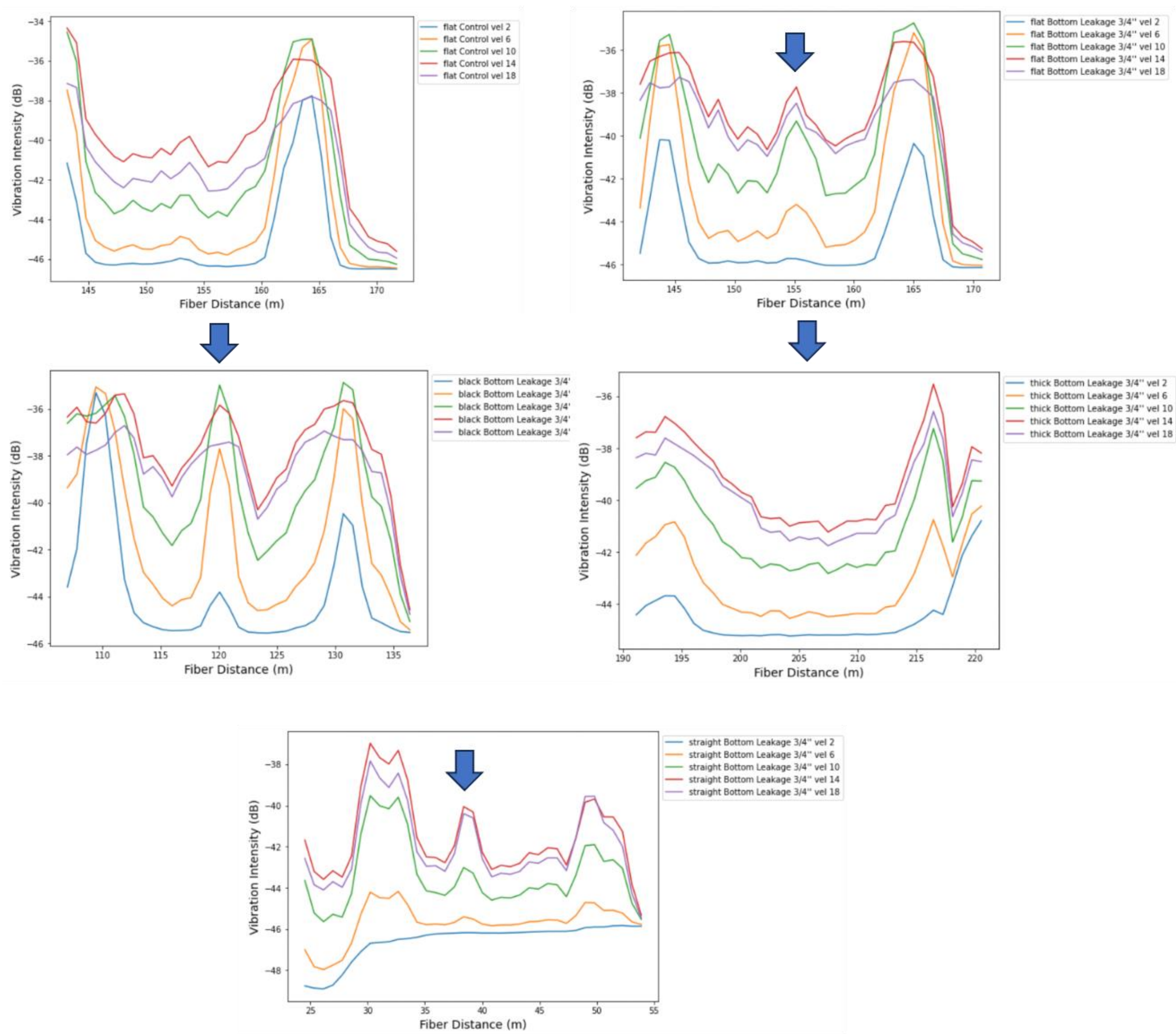

Figure 20. This figure compares the leakage detection sensitivity across different cable types at varying flow velocities. Top left shows a flat cable without leakage as a control experiment. Top right features a flat cable with a leakage hole size of 3/4 inch. The middle left, middle right, and bottom sections present the black, thick, and straight cables with the same leakage size, respectively.

To better understand the cable vibrations induced by leakage, we conducted a Fourier spectrum analysis on the DAS measurements. The primary objective of this analysis is to identify the frequency range associated with the leakage-related signals. Acquiring this information will aid in optimizing leakage detection algorithms and refining future data acquisition parameters. The resulting spectra are organized as 2D arrays, where each column represents the spectrum amplitude for a specific frequency and each row corresponds to the amplitude spectrum for an individual channel.

Figure 21 illustrates the 2-D spectra obtained from experiments involving various leakage sizes at the bottom of a pipe with a flow rate of 10 m/s. High amplitude spectra are conspicuously evident near the leakage points (indicated by blue arrows in Figure 21) for most cases involving straight, black and flat cables. However, the leakage point is less identifiable in the spectra of thicker cables.

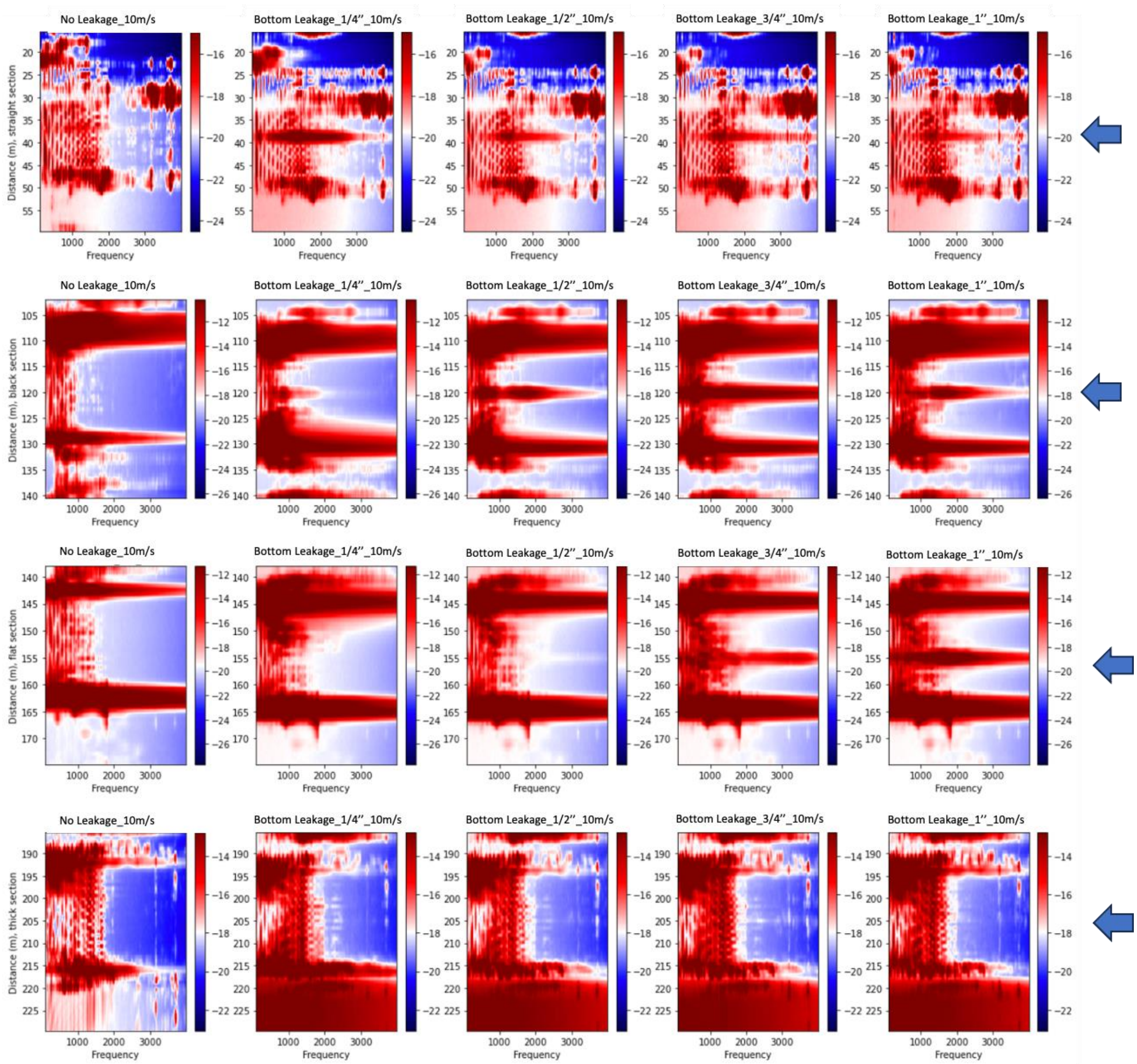

Figure 21. 2D spectra of fiber sections with varying leakage hole sizes at the bottom of the pipe, measured at a flow rate of 10 m/s. The top row displays the straight cable section, followed by the black, the flat, and the thick cable sections. Columns from left to right represent the control experiment (no leakage), followed by leakage sizes of ¼", ½", ¾", and 1", respectively. The color scale is measured in dB. Blue arrows show the leakage point location.

To visualize the amplitude spectrum induced by the leakage more clearly, we extracted the amplitude values corresponding to the leakage location from the 2D spectra and plotted them against frequency. Figure 22 presents the amplitude spectrum for experiments with different leakage sizes, all at a flow rate of 10 m/s. The right column of Figure 22 shows the amplitude ratio between the leakage and control (no leakage) experiments. Our findings indicate that the vibrational anomalies caused by leakage span a broad spectrum. For black cable, we observed up to a 10 dB increase in amplitude across most of the measured frequency range at the leakage point compared to the no-leakage scenario.

The spectral responses appear to be more complex for flat cable. For instance, with leakage sizes of ¼" and ¾", amplitude increases are more uniformly distributed across the entire frequency band, averaging between 1-2 dB. Conversely, for ½" and 1" leakage sizes, the amplitude increases are predominantly concentrated in the 1000-2000 Hz range, exceeding an average of 5 dB. This complex response to leakage is likely due to the flow interactions between the flat cable and the flow deviating from the main pipe into the leakage pathway. Similarly, the straight cable exhibits an amplitude increase concentrated in the same frequency range (1000-2000Hz range). In contrast, little amplitude increase can be observed on the thick cable, which is consistent with the STD results. At large leakage sizes, amplitude increase can be observed at a narrower frequency band, with 600-800 Hz for the ¾’’ leakage size and 1100-1300 Hz for the 1" leakage size.

From the results, we found that the black cable seems to provide more reliable differentiation between leakage and control experiments, which could potentially lead to more reliable leakage detection.

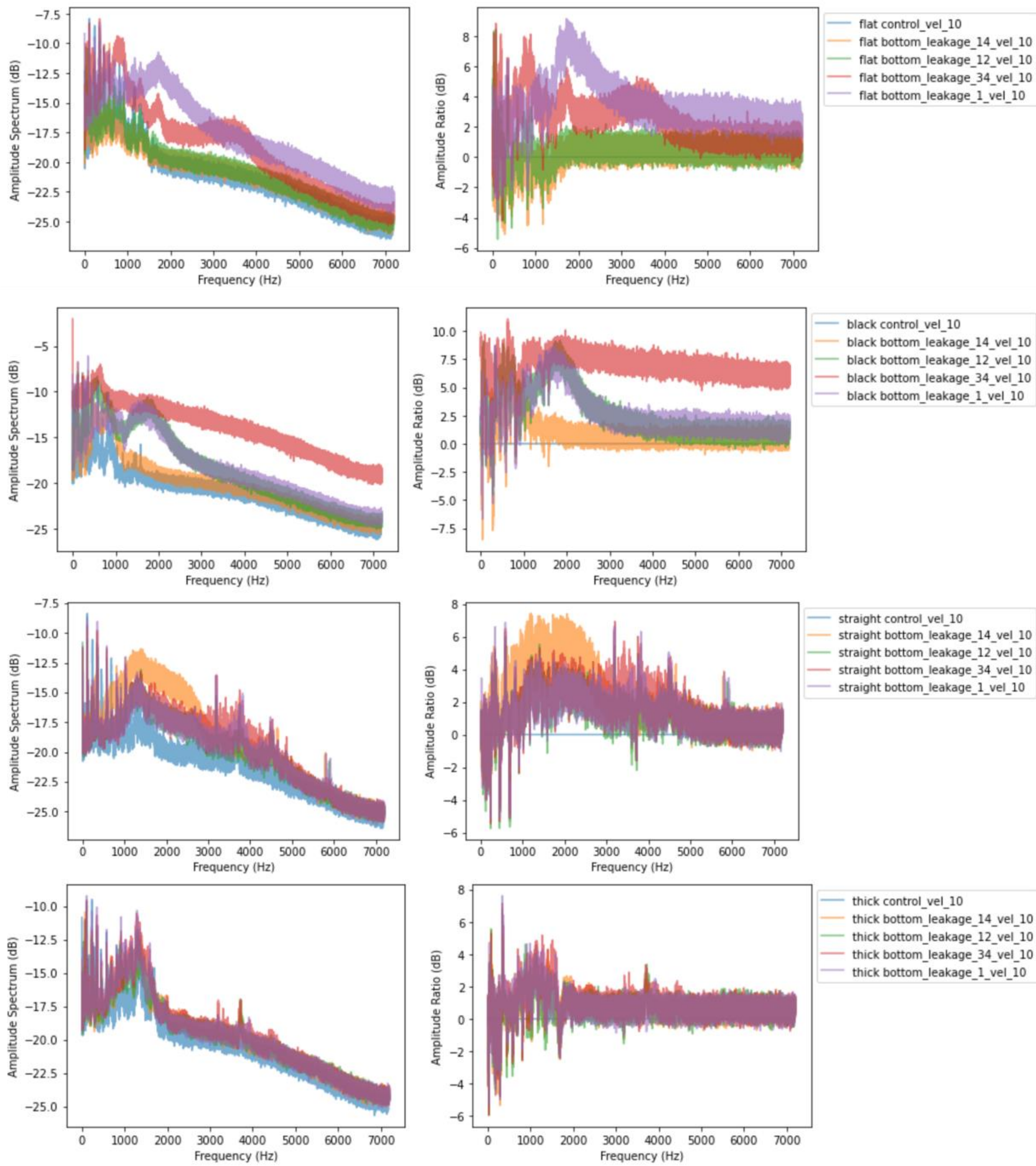

Figure 22. Amplitude spectrum at leakage point locations for various cables and leakage sizes. The flow rate is 10 m/s. The first row displays results for flat cable, the second row for black cable, the third row for the straight cable, and the forth row for thick cable. The left column shows the amplitude spectrum, while the right column presents the ratio of amplitude spectrum between leakage experiments and the control experiment. All values are expressed in decibels (dB).

4. Future work

In the next quarter, we plan to:

1) Complete the experiments for unburied pipe for Task#3;

2) Start the experiments for Tasks#3, #4, and #6 for the buried pipe configuration.

Since the facility preparation is almost ready for the unburied and buried pipeline configuration, we are optimistic that we can finish the experiments on time, given the extension.

References

1. PHMSA: Stakeholder communications - smart pig fact sheet. https://primis.phmsa.dot.gov/comm/FactSheets/FSSmartPig.htm?nocache=4003.
2. Zhang, S., Liu, B. & He, J. Pipeline deformation monitoring using distributed fiber optical sensor. *Measurement (Lond.)* **133**, 208–213 (2019).
3. Hydrotesting effects-1 model predicts crack growth and material behavior. *Oil & Gas Journal* https://www.ogj.com/pipelines-transportation/pipelines/article/17213913/hydrotesting-effects-1-model-predicts-crack-growth-and-material-behavior (1990).
4. Werner, S. Catastrophic failure during Hydro testing. https://wermac.org/misc/pressuretestingfailure4.html.
5. Tajuddin, A. Hydro test Safety - hazards and control measures. *Safety Notes* https://www.safetynotes.net/hydro-test-safety/ (2019).
6. Inaudi, D. & Glisic, B. Long-range pipeline monitoring by distributed fiber optic sensing. *J. Press. Vessel Technol.* **132**, 011701 (2010).
7. Muggleton, J. M., Hunt, R., Rustighi, E., Lees, G. & Pearce, A. Gas pipeline leak noise measurements using optical fibre distributed acoustic sensing. *Journal of Natural Gas Science and Engineering* **78**, 103293 (2020).
8. Nikles, M. *et al.* Leakage detection using fiber optics distributed temperature monitoring. *Smart Structures and Materials 2004: Smart Sensor Technology and Measurement Systems* Preprint at https://doi.org/10.1117/12.540270 (2004).
9. Grosswig, S., Hurtig, E., Luebbecke, S. & Vogel, B. Pipeline leakage detection using distributed fibre optical temperature sensing. *17th International Conference on Optical Fibre Sensors* Preprint at https://doi.org/10.1117/12.623803 (2005).
10. Ukil, A., Libo, W. & Ai, G. Leak detection in natural gas distribution pipeline using distributed temperature sensing. *IECON 2016 - 42nd Annual Conference of the IEEE Industrial Electronics Society* Preprint at https://doi.org/10.1109/iecon.2016.7793562 (2016).
11. Jiang, T., Ren, L., Jia, Z.-G., Li, D.-S. & Li, H.-N. Pipeline internal corrosion monitoring based on distributed strain measurement technique. *Struct. Contr. Health Monit.* **24**, e2016 (2017).
12. Ravet, F., Niklès, M. & Rochat, E. A Decade of Pipeline Geotechnical Monitoring Using Distributed Fiber Optic Monitoring Technology. in *ASME 2017 International Pipeline Geotechnical Conference* (American Society of Mechanical Engineers Digital Collection, 2017). doi:10.1115/IPG2017-2503.
13. Tejedor, J. *et al.* A Novel Fiber Optic Based Surveillance System for Prevention of Pipeline Integrity Threats. *Sensors* **17**, (2017).
14. Stajanca, P. *et al.* Detection of Leak-Induced Pipeline Vibrations Using Fiber-Optic Distributed Acoustic Sensing. *Sensors* **18**, (2018).
15. Blevins, R. D. *Flow-Induced Vibration*. (1977).
16. Sarpkaya, T. *Vortex-Induced Oscillations A Selective Review*. http://www.asme.org/about-asme/terms-of-use (1979).
17. Yang, B., Gao, F.-P., Jeng, D.-S. & Wu, Y.-X. Experimental study of vortex-induced vibrations of a pipeline near an erodible sandy seabed. *Ocean Eng.* **35**, 301–309 (2008).
18. Naudascher, E. & Rockwell, D. *Flow-Induced Vibrations: An Engineering Guide*.

(Courier Corporation, 2012).